Experimental study on needle insertion force to minimize tissue deformation in tongue tissue

Aaboubout, Y.; Nunes Soares, M. R.; Barroso, E. M.; van der Sar, L. C.; Bocharnikov, A.; Usenov, I.; Artyushenko, V.; Caspers, P. J.; Koljenović, S.; Bakker Schut, T. C.

DOI
10.1016/j.medengphy.2021.10.003

Publication date
2021

Document Version
Final published version

Published in
Medical Engineering and Physics

Medical Engineering and Physics 97 (2021) 40–46

Contents lists available at ScienceDirect

Medical Engineering and Physics

journal homepage: www.elsevier.com/locate/medengphy

Experimental study on needle insertion force to minimize tissue deformation in tongue tissue

Y. Aaboubout [a,b,*], M.R. Nunes Soares [a], E.M. Barroso [a,c,d], L.C. van der Sar [a], A. Bocharnikov [e], I. Usenov [e], V. Artyushenko [e], P.J. Caspers [d], S. Koljenović [a], T.C. Bakker Schut [d], J. J. van den Dobbelsteen [f], G.J. Puppels [d]

[a] Department of Pathology, Erasmus MC, University Medical Center Rotterdam, Wytemaweg 80 CN, Rotterdam 3015, the Netherlands
[b] Department of Otorhinolaryngology and Head and Neck Surgery, Erasmus MC, University Medical Center Rotterdam, the Netherlands
[c] Department of Oral and Maxillofacial Surgery, Erasmus MC, University Medical Center Rotterdam, the Netherlands
[d] Department of Dermatology, Erasmus MC, University Medical Center Rotterdam, the Netherlands
[e] Art Photonics GmbH, Berlin, Germany
[f] Department of Biomechanical Engineering, Delft University of Technology, Delft, the Netherlands

ARTICLE INFO

Keywords:
Needle-tissue interaction
Tissue deformation
Oral cavity
Intraoperative assessment
Raman spectroscopy
Head and neck cancer

ABSTRACT

This study reports on the effects of insertion velocity, needle tip geometry and needle diameter on tissue deformation and maximum insertion force. Moreover, the effect of multiple insertions with the same needle on the maximum insertion force is reported. The tissue deformation and maximum insertion force strongly depend on the insertion velocity and the tip geometry. No correlation was found between the outer diameter and the maximum insertion force for small needles (30G – 32G). The endurance experiments showed no remarkable difference in the maximum insertion force during 100 insertions.

1. Introduction

Each year, more than 350.000 new cases of oral cavity cancer are diagnosed, with a mortality rate of >175.000 per year [1]. Squamous cell carcinoma (SCC) counts for 90% of the cancers of the oral cavity [2]. The primary treatment for this type of cancer is surgery. The goal of surgery is the complete removal of the tumor with an adequate resection margin (> 5 mm of healthy tissue surrounding the tumor). Resection margins are an important prognostic factor. Patients with adequate resections have less local recurrence of the tumor and improved overall survival [3–9].

However, achieving adequate resections is often hard due to the complex anatomy of the oral cavity. The surgeon can only rely on visual inspection, palpation, and preoperative imaging during surgery. Recent studies showed that this approach led to adequate resections in only 15–26% of all cases [10–12].

The number of adequate resections can be increased by performing intraoperative assessment of the resection margins [9,13]. At our institute, we perform intraoperative assessment based on visual inspection, palpation, and grossing of the freshly resected specimen, supported by frozen sections when needed [14]. However, this method is labor-intensive and subjective. Therefore, there is a need for an objective intraoperative tool to improve the rate of adequate resections in oral cavity squamous cell carcinoma (OCSCC) patients.

Healthy tissue and tumor have different molecular compositions that can be distinguished by Raman spectroscopy [15]. Raman spectroscopy is a non-destructive optical technique that may allow for (real-time) intraoperative assessment of the molecular composition of tissues. Therefore, we aim for the development of a device with a fiber-optic needle probe that can determine the resection margin based on Raman spectroscopy. The fiber-optic needle is driven into the resection specimen, from the resection surface towards the tumor, while the probe collects Raman signal continuously along the insertion path. By performing multiple insertions on the resection specimen, a complete assessment of all resection margins is possible.

With the Raman fiber-optic needle probe, we aim to determine the distance between the resection surface and the tumor border with a maximum error of 1 mm. Tissue deformation during needle insertion is one potential source of error, which we want to limit to $\leq$ 0.5 mm leaving 0.5 mm due to other potential sources of error. Moreover, for a

* Corresponding author at: Department of Pathology, Erasmus MC, University Medical Center Rotterdam, Wytemaweg 80 CN, Rotterdam 3015, the Netherlands.
E-mail address: y.aaboubout@erasmusmc.nl (Y. Aaboubout).

https://doi.org/10.1016/j.medengphy.2021.10.003
Received 9 June 2021; Received in revised form 13 September 2021; Accepted 4 October 2021
Available online 6 October 2021

complete assessment of all resection margins of a specimen, multiple insertions (up to 100 times) are required, which might lead to deterioration of the needle and affect measurement accuracy. The main intent of this study is to gain insight into tissue deformation during needle insertion including the effect of multiple insertions.

Needle–tissue interaction is well described in the literature [16–18]. The needle insertion is divided into 3 phases, namely boundary displacement, tip insertion, and tip and shaft insertion [18]. The boundary displacement phase starts with the needle making contact with the tissue boundary and ends with the puncturing event (breaching of the surface of the tissue). During this phase, the force and tissue deformation continues to grow until the end of the phase. The tip insertion phase starts with the breaching of the surface of the tissue and ends with the tissue surface sliding from the tip onto the shaft of the needle. This coincides in most cases with a drop of the force. The tip and shaft insertion phase starts after the tissue surface moved over the needle tip onto the shaft of the needle (the needle entered the tissue with the tip and first part of the shaft). This phase ends either with the needle being stopped or a new boundary is encountered internally in the tissue. These phases will be recurrent if different tissue properties or multiple internal structures are encountered during the needle insertion [18].

The literature shows that force and tissue deformation are highly influenced by: (1) needle characteristics (diameter, tip geometry, coating, others), (2) insertion method (insertion velocity, drive mode, insertion process), and (3) tissue characteristics [16,18]. All of these factors need to be taken into account when optimizing the proposed fiber-optic needle probe for intraoperative assessment. Specific studies on needle-tissue interaction in oral cavity tissue or phantoms/biologic materials that mimic the oral cavity are however lacking. In the current study, we therefore investigate the effect of needle velocity and needle characteristics on the deformation of tongue tissue during needle insertions. We also report on the effect of multiple insertions on the needle insertion force.

2. Methods and materials

2.1. Tested needles

Eight commercial needles (specified in Table 1), with different tip geometries and outer diameters, were selected for this study.

2.2. Tested materials

Calf tongue was used for testing, because of its similarity to the human tongue. The tongue is the most prevalent location for OCSCC [9,19,20]. Tissue blocks of 2 cm × 2 cm × 2 cm were cut from a fresh calf tongue, to fit the transparent measurement container (Fig. 1B). The tissue blocks always originated from the center of the tongue dorsum (Fig. 1A).

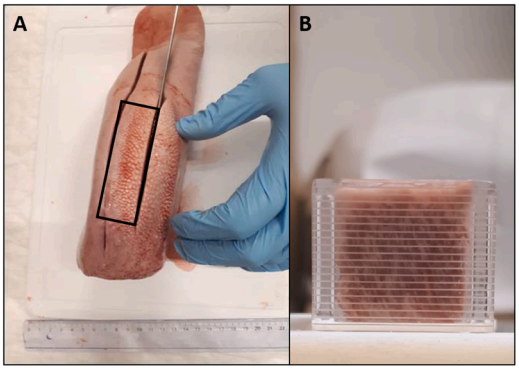

Fig. 1. Calf tongue used for experiments. A. Cutting of the calf tongue, the black square indicates the area that was used for the experiments. B. Tissue blocks of 2 cm × 2 cm × 2 cm in the transparent measurement container with engraved horizontal lines with a spacing of 1 mm.

2.3. Experimental setup

A force setup developed at the Faculty of Mechanical Engineering and Biomechanical Engineering at the Delft University of Technology was used to measure the maximum insertion force (Fig. 2). The experimental setup consists of a linear stage (EGSL-BS-45-200-3P, Festo BV, Delft, The Netherlands) that moves in a vertical direction. Attached to the linear stage are a needle holder and an S-Beam Load Cell sensor (LSB200-FSH00104, FUTEK Advanced Sensor Technology Inc., Irvine, CA, USA). This sensor can register tension forces and compression forces. The sensor can read forces in the range of 0 to 10lbs (44.5 N). Four stage velocities (1 mm/s, 5 mm/s, 10 mm/s, and 20 mm/s) can be selected. The force sensor setup uses a MatLab interface for control and data acquisition.

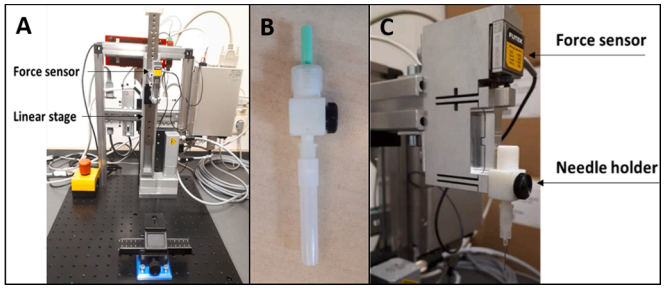

Fig. 2. The setup to measure the insertion force. A. The force sensor is attached to a linear stage. B. The needle holder consisting of a Luer Lock (bottom part) and a 'Universal Lock' (top part). C. The needle holder is attached to the force sensor.

Table 1
List of needles.

Label	Type	Gauge	Ø(mm)	Tip shape	Material	Lubricant
3FB-Sterican 26G	Sterican*	26G	0.45	3 facet bevel	Stainless chromium nickels steel	Light silicone coating
3FB-Sterican 27G	Sterican*	27G	0.40	3 facet bevel	Stainless chromium nickels steel	Light silicone coating
3FB-Sterican 30G	Sterican*	30G	0.30	3 facet bevel	Stainless chromium nickels steel	Light silicone coating
Blunt-Sterican 27G	Sterican*	27G	0.40	Blunt (90°)	Stainless chromium nickels steel	Light silicone coating
3FB-Omnican 30G	Omnican*	30G	0.30	3 facet bevel	Stainless chromium nickels steel	Light silicone coating
38B-Omnican 30G	Omnican**	30G	0.30	bevel 38°	Stainless chromium nickels steel	Light silicone coating
Diamond-Clickfine 31 G	Clickfine***	31G	0.25	Diamond tip	Stainless steel	-
Diamond-Clickfine 32 G	Clickfine***	32G	0.23	Diamond tip	Stainless steel	-

* Produced by B. Braun Holding GmbH & Co KG, Melsungen, Germany
** Produced by B. Braun Holding GmbH & Co KG, Melsungen, Germany and adjusted to 38° bevel by art photonics GmbH, Berlin, Germany
*** Produced by Ypsomed AG, Burgdorf, Switzerland

2.4. Insertion protocol

Each needle was inserted into the tissue blocks at four different velocities: 1 mm/s, 5 mm/s, 10 mm/s, and 20 mm/s. To obtain a minimum required Raman signal quality the signal collection time should at least be 50–100 ms (based on other experiments). To achieve an accuracy of 1 mm for the determination of the margin a Raman measurement is needed every 0.5 mm (in accordance with the Nyquist theorem). This means that the maximum insertion velocity is 10 to 20 mm/s. We have also explored lower insertion velocities because this would allow longer Raman signal collection time and further improve Raman signal quality. For each velocity, five different insertions were performed. The needle was inserted perpendicularly to the tissue surface. To visualize tissue deformation, the insertions were performed close to the walls of the measurement containers. The needle was inserted each time at a different tissue location. For each needle, a new tissue block was used.

The measurement container has a scale that consists of engraved horizontal lines with a spacing of 1 mm. This scale was used to measure tissue deformation. A camera was placed next to the container and each insertion was video recorded to determine the deformation. Deformation was defined as the deepest point of tissue compression visible on the engraved raster on the measurement container. The average tissue deformation (mm) was calculated per needle and insertion velocity.

The needles with a deformation $\leq$ 0.5 mm were selected for the endurance experiments. Each selected needle was inserted into tongue tissue up to 100 times using the measurement container. The needle was inserted each time at a different tissue location. The maximum insertion force was collected for each insertion and plotted as a function of the number of insertions. The endurance experiments were performed with the best performing insertion velocities (10 mm/s and 20 mm/s) based on the first set of experiments.

2.5. Data processing

During needle insertion, the sensor signal (voltage) was recorded as a function of time. The voltage readings were converted into force (N) using a set of calibration measurements. Five calibration discs with known masses (93.8 g, 69.5 g, 43.3 g, 21.1 g, 0 g) were used. The voltage induced in the sensor by each disc was recorded while the disc was hanging from the needle holder and plotted as a function of the force exerted by the disk (Fig. 3). A first-order polynomial regression of calibration data was used to convert the voltage to force (N): $V = 0.12 \times F - 4.87$ (Fig. 3).

For this study, the maximum insertion force was considered to evaluate and compare the performance of the needles. The maximum force (N) of each needle insertion was determined by finding the maximum value in the force curve (Fig. 4). The maximum forces of the 5

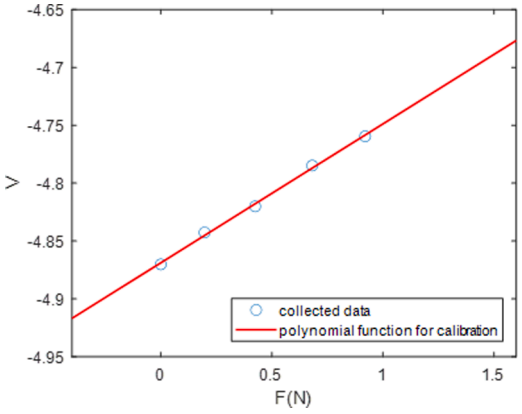

Fig. 3. Graphical representation of voltage as a function of force (N) and polynomial approximation: $V = 0.12*F - 4.87$.

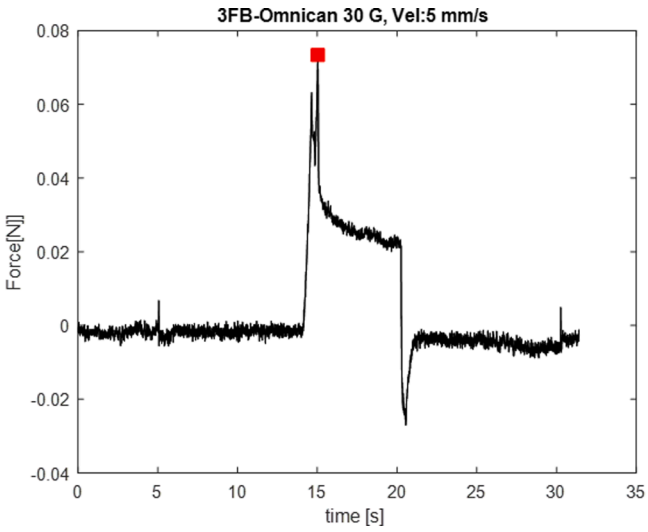

Fig. 4. Example of the maximum value (red dot) of the force of needle insertion in tongue tissue.

insertions performed with the same needle and with the same velocity were averaged.

3. Results

Fig. 5 shows the force profiles (insertion force as a function of time) on the needle during insertions in tongue tissue at a velocity of 5 mm/s. What can be observed is that, after the needle touches the tissue, there is an increase in the insertion force until the tissue surface is punctured. After the puncture, there is a decrease in the insertion force. For most of the tested needles, the insertion is accompanied by multiple puncture events that can be identified by several peaks in the force profile.

Fig. 6A shows tissue deformation and maximum insertion force for all tested needles, at different insertion velocities. The values of deformation and maximum force are averages of 5 insertions. The needle with blunt tip geometry (see also Fig 5D) showed a much higher insertion force and tissue deformation than other needles. Fig. 6B zooms in on the other seven needle types.

The remaining needles (3FB-Omnican 30G, 38B-Omnican 30G, Diamond 31G, and Diamond 32G) show the lowest insertion force.

The effect of increasing insertion velocity on the tissue deformation for these four needles is illustrated in Fig. 6C. Clearly, a higher insertion velocity results in a decrease in tissue deformation.

The performance of pre-selected needles (3FB-Omnican 30G, 38B-Omnican 30G, Diamond-Clickfine 31G, and Diamond-Clickfine 32G) was further evaluated in an endurance test. It consisted of up to 100 consecutive insertions of a needle in tongue tissue while recording the insertion force. The maximum force was determined for each insertion and plotted as a function of the insertion number. The results are shown in Fig. 7. The endurance test was performed at two insertion velocities: 10 mm/s (blue) and 20 mm/s (red). For each of the four needle types, the maximum insertion force remains constant during the endurance tests.

4. Discussion

Our study aimed to gain insights into tissue deformation during the insertion of a needle into tongue tissue and the effect of multiple insertions. This study showed that the tissue deformation and the maximum insertion force strongly depend on the tip geometry and the insertion velocity. Moreover, the endurance experiments showed no notable difference in the maximum insertion force during 100 insertions.

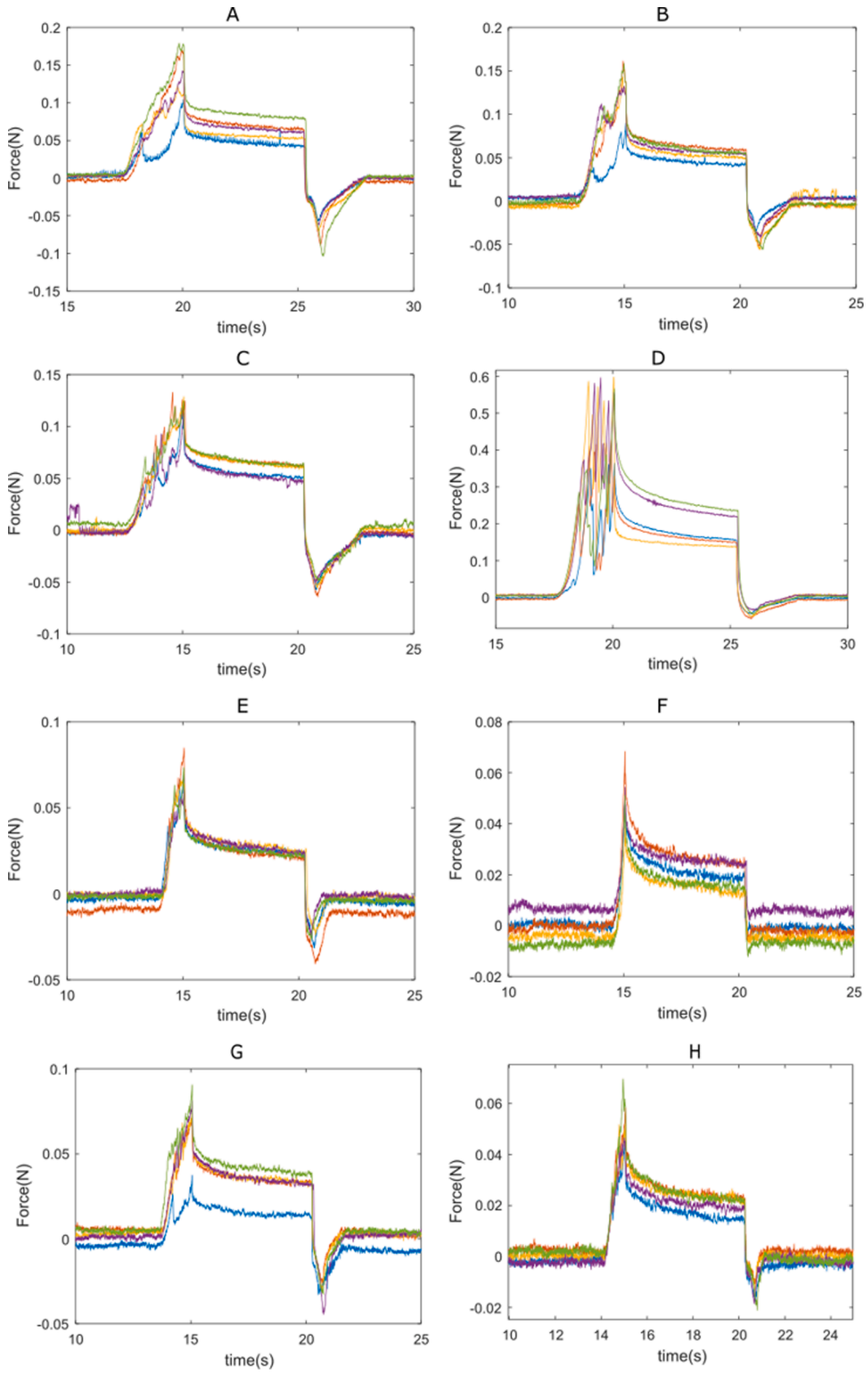

Fig. 5. Typical insertion force profiles for each of the eight tested needle types, obtained for an insertion velocity of 5 mm/s. A. 3FB-Sterican 26G; B. 3FB-Sterican 27G; C. 3FB-Sterican 30G; D.Blunt 27G; E. 3FB-Omnican 30G; F. 38B-Omnican 30G; G. Diamond-Clickfine 31G; H Diamond-Clickfine 32G

For the intended application, tissue deformation should be limited to $\leq$ 0.5 mm. In our experiments, four needles (3FB-Omnican 30G, 38B-Omnican 30G, Diamond-Clickfine 31G, and Diamond-Clickfine 32G) met this requirement at high velocities (10 mm/s and 20 mm/s). However, in the system under development, the maximum insertion velocity should be limited to about 5 mm/s to allow longer Raman signal collection time and further improve Raman signal quality. Only one needle (38B-Omnican 30G) met our requirement of $\leq$ 0.5 mm deformation at a velocity of 5 mm/s.

Throughout the experiments, multiple puncturing events were recognized, as shown in Fig. 5. This is a well-described effect in the literature for biological tissue [21,22]. The multiple puncturing events are most likely due to the different orientations of the muscle fibers of the calf tongue. In most cases, the maximum insertion force does not

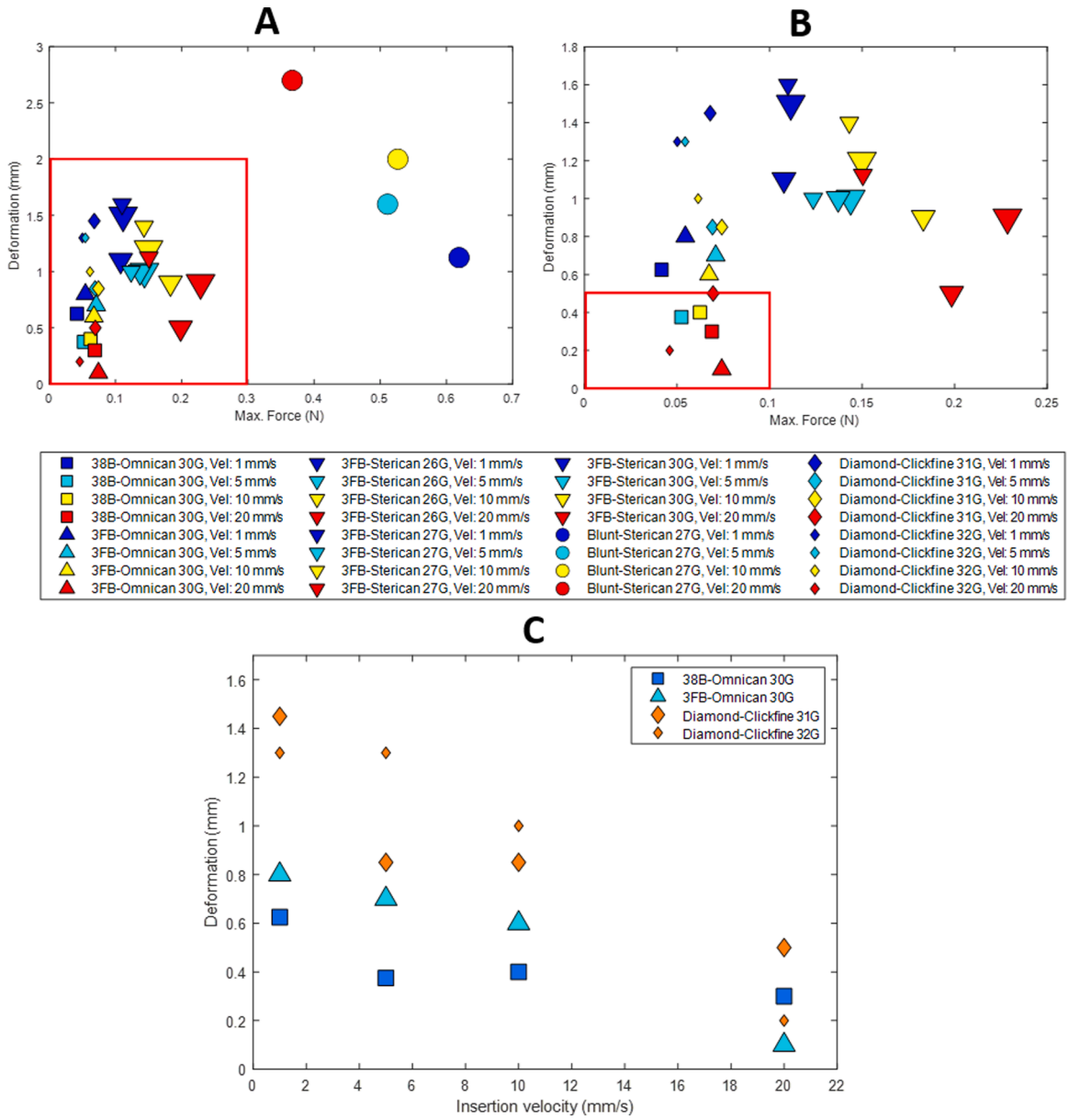

Fig. 6. The size of the symbols is correlated with the diameter of the needles. A. Deformation versus maximum insertion force for all insertion velocities and needles. B. Showing all needles in the red rectangle of A, excluding the needle with the blunt tip geometry. C. Deformation as a function of insertion velocity for the needles that showed the lowest deformation and lowest maximum insertion force in the red rectangle of B.

correspond to the tissue surface puncture force, but to a puncture event that occurs inside the tissue. Before the puncture event, the tissue is pushed away by the needle tip, resulting in tissue deformation and an increase in force. For our intended application of fiber-optic needles, it is important to minimize tissue deformation both at the tissue surface and inside the tissue.

In the system under development, a single needle will be used for the assessment of tumor resection margins at many locations of the resected tissue. This means that the needle must endure multiple insertions in soft tissue. All of the selected commercial needles are intended for single use only. Reports have shown that a needle tip can deteriorate after multiple insertions, which might lead to an increase in the maximum insertion force [23,24]. We tested this but did not observe an increase of insertion force during 100 insertions in tongue tissue. This might be due to the tissue characteristics of calf tongue and the design of the tested needles (3FB-Omnican 30G, 38B-Omnican 30G, Diamond-Clickfine 31G, and Diamond-Clickfine 32G). Moreover, in the endurance experiments, 3 of the 4 needles show essentially no difference in the insertion force between 10 and 20 mm/s. The exception is the 3FB-Omnican 30G needle which shows a markedly, not yet understood, higher insertion force for the 10 mm/s.

The literature shows that the tip geometry is an important determining factor for the insertion force [18,25–27]. Hirsch et al. showed that by adding 2 cutting edges (5 facet bevel instead of 3 facet bevel), the puncture force could be reduced by 23% [28]. This was also observed in this work, the needles with a blunt tip performed the worst followed by the 3FB-Sterican needles. Even for needles with a similar tip shape such as the 3FB-Omnican and 3FB-Sterican we observed a difference in the insertion force, which is possibly due to the angles of the tip. A smaller maximum force and a smaller deformation were observed for the 3FB-Omnican 30G in comparison to the 3FB-Sterican 30G. The diamond tip needles that were included in this study, are 6 facet beveled needles. However, the 3 facet beveled and the 38° beveled needles performed equally well or better than the diamond tip needles.

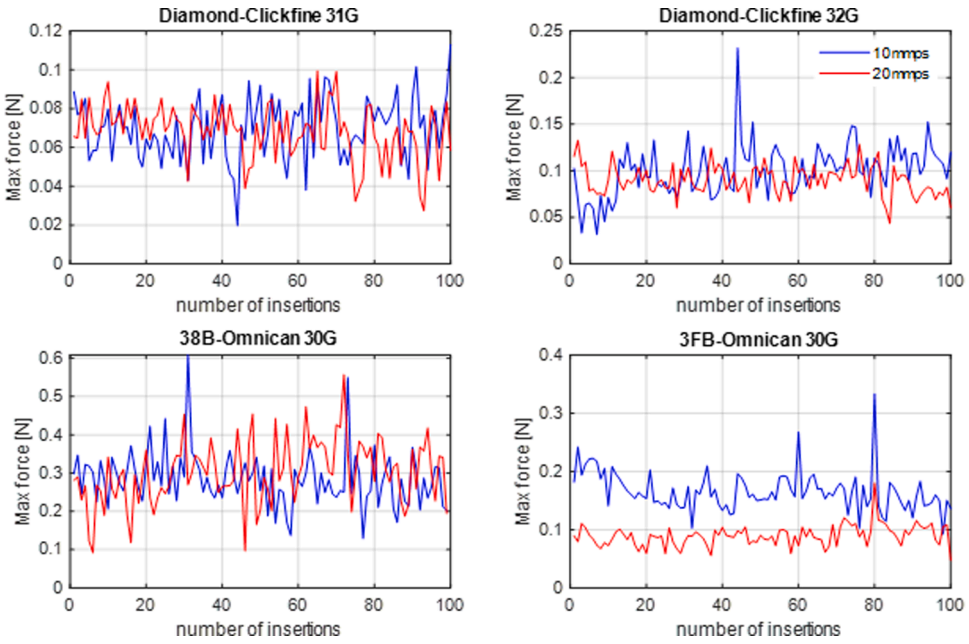

Fig. 7. Maximum insertion force as a function of the number of consecutive needle insertions in tongue tissue for the four needle types and two insertion velocities (10 mm/s (blue) and 20 mm/s (red)).

To visualize and measure the tissue deformation, the needles were inserted 3 mm from the wall of the measuring cubes. This could possibly affect the boundary conditions compared to real *ex-vivo* experiments and thereby change tissue deformation and insertion force. However, we do not expect that this will affect our conclusions with respect to the most suitable needle and insertion velocity given the very small deformation that was observed.

According to the literature, the force needed to create a puncture event increases with the needle's outer diameter [16]. In the current study, we examined a set of needles with small diameters (26G – 32G) compared to the ones studied in the literature (7 G to 30 G) [16]. However, for the thinnest needles (30G – 32G), no correlation between insertion force and needle diameters was found.

The insertion velocity had a great impact on tissue surface deformation, which supports the literature [29]. Fig. 6C shows that the deformation decreases with the increase of the insertion velocity, which was the case for nearly all needles. However, only four different insertion velocities (1 mm/s, 5 mm/s, 10 mm/s, and 20 mm/s) were tested and more insertion velocities should be investigated in the future. Moreover, to optimize needles for any intended application and any biological tissue, future research should focus on selecting comparable biological tissue and selecting needles with different tip geometries.

5. Conclusions

This study showed that the tissue deformation and the maximum insertion force strongly depend on the tip geometry and the insertion velocity for needles with a small outer diameter (30G – 32G). An increase in the insertion velocity decreases tissue deformation. Moreover, the needle tip geometry is an important factor to consider when optimizing the needle for any intended application. Of all the tested needles in this study, the 3FB-Omnican 30G and 38B-Omnican 30G needles performed the best in tongue tissue in regards to the maximum insertion force and tissue deformation. The needles selected for the endurance test showed no notable difference in the maximum insertion force during 100 insertions. Based on these outcomes the 38B-Omnican 30G needle was selected for the device under development Fig. 7.

Funding

This research received funding from the Dutch Cancer Society (Project 106467 - Optimizing surgical results for oral squamous cell carcinoma by intra-operative assessment of resection margins using Raman spectroscopy) and Eurostars E (Project 12076 – RA-SURE).

Ethical approval

Not required.

Declaration of Competing Interest

None to declare.

References

[1] Ferlay J, Soerjomataram I, Dikshit R, Eser S, Mathers C, Rebelo M, et al. Cancer incidence and mortality worldwide: sources, methods and major patterns in GLOBOCAN 2012. Int J Cancer 2015;136:E359–86. https://doi.org/10.1002/ijc.29210.

[2] Vigneswaran N, Williams MD. Epidemiologic trends in head and neck cancer and aids in diagnosis. Oral Maxillofac Surg Clin N Am 2014;26:123–41. https://doi.org/10.1016/j.coms.2014.01.001.

[3] Helliwell T.R., Woolgar J.A., Royal college of pathologists publications 2013.

[4] Dillon JK, Brown CB, McDonald TM, Ludwig DC, Clark PJ, Leroux BG, et al. How does the close surgical margin impact recurrence and survival when treating oral squamous cell carcinoma? J Oral Maxillofac Surg 2015;73:1182–8. https://doi.org/10.1016/j.joms.2014.12.014.

[5] Slootweg PJ, Hordijk GJ, Schade Y, van Es RJJ, Koole R. Treatment failure and margin status in head and neck cancer. A critical view on the potential value of molecular pathology. Oral Oncol 2002;38:500–3. https://doi.org/10.1016/s1368-8375(01)00092-6.

[6] Al-Rajhi N, Khafaga Y, El-Husseiny J, Saleem M, Mourad W, Al-Otieschan A, et al. Early stage carcinoma of oral tongue: prognostic factors for local control and survival. Oral Oncol 2000;36:508–14. https://doi.org/10.1016/S1368-8375(00)00042-7.

[7] Binahmed A, Nason RW, Abdoh AA. The clinical significance of the positive surgical margin in oral cancer. Oral Oncol 2007;43:780–4. https://doi.org/10.1016/j.oraloncology.2006.10.001.

[8] Loree TR, Strong EW. Significance of positive margins in oral cavity squamous carcinoma. Am J Surg 1990;160:410–4. https://doi.org/10.1016/s0002-9610(05)80555-0.

[9] Smits RWH, van Lanschot CGF, Aaboubout Y, de Ridder M, Hegt VN, Barroso EM, et al. Intraoperative assessment of the resection specimen facilitates achievement

of adequate margins in oral carcinoma. Front Oncol 2020;10:614593. https://doi.org/10.3389/fonc.2020.614593.
[10] Varvares MA, Poti S, Kenyon B, Christopher K, Walker RJ. Surgical margins and primary site resection in achieving local control in oral cancer resections. Laryngoscope 2015;125:2298–307. https://doi.org/10.1002/lary.25397.
[11] Smits RWH, Koljenović S, Hardillo JA, ten Hove I, Meeuwis CA, Sewnaik A, et al. Resection margins in oral cancer surgery: room for improvement: resection margins in oral cancer surgery. Head Neck 2016;38:E2197–203. https://doi.org/10.1002/hed.24075.
[12] Dik EA, Willems SM, Ipenburg NA, Adriaansens SO, Rosenberg A, van Es RJJ. Resection of early oral squamous cell carcinoma with positive or close margins: relevance of adjuvant treatment in relation to local recurrence. Oral Oncol 2014;50:611–5. https://doi.org/10.1016/j.oraloncology.2014.02.014.
[13] Aaboubout Y, Ten Hove I, Smits RWH, Hardillo JA, Puppels GJ, Koljenovic S. Specimen-driven intraoperative assessment of resection margins should be standard of care for oral cancer patients. Oral Dis 2021;27:111–6. https://doi.org/10.1111/odi.13619.
[14] Santos IP, Barroso EM, Schut TCB, Caspers PJ, Lanschot CGF, van, Choi DH, et al. Raman spectroscopy for cancer detection and cancer surgery guidance: translation to the clinics. Analyst 2017;142:3025–47. https://doi.org/10.1039/C7AN00957G.
[15] Barroso EM, Smits RWH, Bakker STC, ten Hove I, Hardillo JA, Wolvius EB, et al. Discrimination between oral cancer and healthy tissue based on water content determined by Raman spectroscopy. Anal Chem 2015;87:2419–26. https://doi.org/10.1021/ac504362y.
[16] Jiang S, Li P, Yu Y, Liu J, Yang Z. Experimental study of needle-tissue interaction forces: effect of needle geometries, insertion methods and tissue characteristics. J Biomech 2014;47:3344–53. https://doi.org/10.1016/j.jbiomech.2014.08.007.
[17] Bao X, Li W, Lu M, Zhou ZR. Experiment study on puncture force between MIS suture needle and soft tissue. Biosurf Biotribol 2016;2:49–58. https://doi.org/10.1016/j.bsbt.2016.05.001.
[18] van Gerwen DJ, Dankelman J, van den Dobbelsteen JJ. Needle-tissue interaction forces–a survey of experimental data. Med Eng Phys 2012;34:665–80. https://doi.org/10.1016/j.medengphy.2012.04.007.
[19] van Lanschot C, Klazen YP, de Ridder M, Mast-Kramer H, Ten HI, Hardillo J, et al. Depth of invasion in early stage oral cavity squamous cell carcinoma: the optimal cut-off value for elective neck dissection. Oral Oncol 2020;111. https://doi.org/10.1016/j.oraloncology.2020.104940.
[20] Aaboubout Y, van der Toom QM, de Ridder MAJ, De Herdt MJ, van der Steen B, van Lanschot CGF, et al. Is the depth of invasion a marker for elective neck dissection in early oral squamous cell carcinoma? Front Oncol 2021;11:628320. https://doi.org/10.3389/fonc.2021.628320.
[21] Mahvash M, Dupont PE. Mechanics of dynamic needle insertion into a biological material. IEEE Trans Biomed Eng 2010;57:934–43. https://doi.org/10.1109/TBME.2009.2036856.
[22] Liu W, Yang Z, Li P, Zhang J, Jiang S. Mechanics of tissue rupture during needle insertion in transverse isotropic soft tissue. Med Biol Eng Comput 2019;57:1353–66. https://doi.org/10.1007/s11517-019-01955-6.
[23] Fonseca CG, Castillo DR, Cristerna BC, Masuoka D, Guillén AP. Bevel tip deformation in new and used dental needles. Microsc Res 2015;3:1–5. https://doi.org/10.4236/mr.2015.31001.
[24] Skapetis T, Doan-Tran PD, Hossain NM. Evaluation of bevelled needle tip deformation with dental inferior alveolar nerve blocks. Aust Endod J Aust Soc Endodontol Inc 2019;45:325–30. https://doi.org/10.1111/aej.12361.
[25] Qi Y, Jin J, Chen T, Cong Q. Modeling of geometry and insertion force of a new lancet medical needle. Sci Prog 2020;103:36850419891074. https://doi.org/10.1177/0036850419891074.
[26] Jushiddi MG, Cahalane RM, Byrne M, Mani A, Silien C, Tofail SAM, et al. Bevel angle study of flexible hollow needle insertion into biological mimetic soft-gel: simulation and experimental validation. J Mech Behav Biomed Mater 2020;111:103896. https://doi.org/10.1016/j.jmbbm.2020.103896.
[27] Abolhassani N, Patel R, Moallem M. Needle insertion into soft tissue: a survey. Med Eng Phys 2007;29:413–31. https://doi.org/10.1016/j.medengphy.2006.07.003.
[28] Hirsch L, Gibney M, Berube J, Manocchio J. Impact of a modified needle tip geometry on penetration force as well as acceptability, preference, and perceived pain in subjects with diabetes. J Diabetes Sci Technol 2012;6:328–35. https://doi.org/10.1177/193229681200600216.
[29] Mahvash M, Dupont PE. Fast needle insertion to minimize tissue deformation and damage. In: Proceedings of the IEEE international conference on robotics and automation; 2009. p. 3097–102. https://doi.org/10.1109/ROBOT.2009.5152617. 2009.